Journal of Alloys and Compounds 606 (2014) 242–248

Contents lists available at ScienceDirect

Journal of Alloys and Compounds

journal homepage: www.elsevier.com/locate/jalcom

Phase equilibria in the neodymium–cadmium binary system

Barbara Skołyszewska-Kühberger, Thomas L. Reichmann, Herbert Ipser *

Department of Inorganic Chemistry (Materials Chemistry), University of Vienna, A-1090 Wien, Austria

ARTICLE INFO

Article history:
Received 10 February 2014
Received in revised form 28 March 2014
Accepted 1 April 2014
Available online 13 April 2014

Keywords:
Nd–Cd alloys
Nd–Cd intermetallic compounds
Microstructure
DTA
Dilatometry

ABSTRACT

The equilibrium phase diagram of the neodymium–cadmium system has been established by thermal, metallographic and X-ray analysis based on a study of 70 alloys. The system contains three congruently melting intermetallic compounds, i.e. NdCd (1040 °C), $NdCd_2$ (995 °C), $Nd_{11}Cd_{45}$ (855 °C), and four incongruently melting compounds $NdCd_3$ (860 °C), $Nd_{13}Cd_{58}$ (740 °C), $NdCd_6$ (655 °C) and $NdCd_{11}$ (520 °C). Four eutectic reactions are found in this binary system, i.e. at ~25 at.% Cd and 770 °C, at 58 at.% Cd and 955 °C, at 79 at.% Cd and 850 °C, and very close to pure Cd at 318 °C, as well as one eutectoid reaction at ~15 at.% Cd and 500 °C. The solid solubility of Nd in Cd is negligible. Dilatometric curves were recorded for three Nd–Cd compositions up to 4 at.% Cd, to accurately determine phase transitions between the solid solutions of Cd in the low- and high-temperature modification of Nd.

1. Introduction

Pyrochemical reprocessing techniques for high burn-up nuclear fuels promise more efficiency than traditional aqueous methods [1,2]. As described by Olander [2], pyrochemical reprocessing is based on an "electro-refining" process where a liquid metal cathode is applied for the selective recovery of Pu and minor actinides (MA). At least three different low-melting metals were investigated for this purpose: Kurata et al. [3] proposed Bi and Cd, and later on Conocar et al. obtained promising results using liquid Al [1]. As rare earth elements (RE) behave chemically in a similar way compared to minor actinides, optimal reprocessing conditions require also a detailed knowledge on the extractability of these elements, as described by Kurata et al. [3]. Accordingly, the formation of RE-Me intermetallic compounds affects the performance of the extraction process. For its optimization and better efficiency the knowledge on the existence and stability of the occurring compounds in the various binary phase diagrams RE-Me is important.

The present study has been carried out as part of a research project on the interaction of different RE elements (Ce, Pr, Nd and Gd) with Cd [4–7]. It presents the phase equilibria in the Nd–Cd system as a function of temperature and composition and specifies the existing Nd–Cd intermetallic compounds as well as all phase reactions among them.

A first partial Nd–Cd phase diagram was reported by Elliot [8] who presented the Cd-rich part for temperatures up to 600 °C. The first more detailed study of the Nd–Cd phase diagram was provided by Iandelli [9,10] who described the crystal structure of four intermetallic compounds, i.e. NdCd, $NdCd_2$, $NdCd_3$ and $NdCd_{11}$, applying X-ray diffraction (XRD). Nevertheless, no information concerning the melting temperatures of these compounds was given. It was later summarized by Gschneidner [11] with additional information about two allotropic modifications of Nd: α-Nd [12] and the high temperature modification β-Nd [13]. Further work in this system was done by Johnson et al. [14,15] who determined the solubility of Nd in liquid Cd by chemical analysis of filtered samples of the equilibrium liquid phase in the temperature range 347–498 °C. The most Cd-rich compound in equilibrium with liquid Cd is $NdCd_{11}$. The peritectic decomposition of this phase at 530 °C was examined for a sample containing about 5 at.% Nd using differential thermal analysis (DTA). A maximum solubility of Nd at this peritectic was calculated as 2.6 at.% [15,16]. The existence of cubic $RECd_6$ was discussed by Johnson et al. [16], and later on the crystal structure of YCd_6, that shows close relationship with $NdCd_6$, was determined [17]. Bruzzone et al. [18] determined the existence and crystal structure of the following Nd–Cd compounds by use of metallographic and X-ray methods: $NdCd_4$ (γ-brass type) and $Nd_2Cd_{9\sim}$ ($Pu_{13}Zn_{58}$ type). The existence of a phase with the $Pu_{13}Zn_{58}$ type structure had been reported earlier by Iandelli and Ferro [19] but only for the La–Cd and Ce–Cd system. A rudimentary phase diagram of the Nd–Cd system can be found in Massalski's handbook [20], based mainly on the earlier work by Johnson et al. [15,16] and on the assessment of Gschneidner and Calderwood [21]. Seven intermetallic compounds are known which were also summarized by Colinet and

* Corresponding author. Tel.: +43 1427752906.
E-mail address: herbert.ipser@univie.ac.at (H. Ipser).

http://dx.doi.org/10.1016/j.jallcom.2014.04.009
0925-8388/

Table 1
Crystal structure data (from literature) of phases in the Nd–Cd system.

Phase	Composition (at.% Cd)	Structure type	Pearson symbol	Space group	Refs.
α-Nd	0–3.0[a]	α-La	*hP4*	$P6_3/mmc$	[12]
β-Nd	0–19.0[a]	W	*cI2*	$Im\bar{3}m$	[13]
NdCd	50.0[b]	CsCl	*cP2*	$Pm\bar{3}m$	[9,10]
$NdCd_2$	66.7[b]	CdI_2	*hP3*	$P\bar{3}m1$	[9,10]
$NdCd_3$	75.0[b]	BiF_3	*cF16*	$Fm\bar{3}m$	[9,10]
$Nd_{11}Cd_{45}$	80.4[b]	γ-brass	*cF448*	$F\bar{4}3m$	[18]
$Nd_{13}Cd_{58}$	81.7[b]	$Pu_{13}Zn_{58}$	*hP142*	$P6_3/mmc$	[18]
$NdCd_6$	85.7[b]	YCd_6	*cI168*	$Im\bar{3}$	[17]
$NdCd_{11}$	91.7[b]	$BaHg_{11}$	*cP36*	$Pm\bar{3}m$	[9,10]

[a] Derived from the present results.
[b] Given by Massalski [20].

Pasturel [22]. Table 1 compiles crystallographic data for all binary compounds and solid solutions that were determined in the Nd–Cd phase diagram.

Veleckis and van Deventer [23] listed temperatures for various "RE-RECd eutectics" obtained experimentally, among them a value of 486 °C for the Nd–Cd system. However, this value is obviously flawed due to the approximation of results derived from the Denbigh equation [21] and is far off the value proposed later in Ref. [20] (about 650 °C).

2. Experimental

The starting materials used to prepare the Nd–Cd alloys were Cd shot (United Mineral & Chemical Corporation, U.S.A., and Alfa Aesar, Karlsruhe, Germany; both 99.9999%) and Nd in form of foil/rod (Alfa Aesar, Karlsruhe, Germany; 99.9%) and pieces (smart-elements, Vienna, Austria, 99.9%). Due to the high reactivity of Nd the preparation procedure was done in a glove box (MBraun Labmaster 130) under an Ar atmosphere (<1 ppm O_2, <1 ppm H_2O). Before use, the Nd pieces were cleaned with a file until a shiny surface was obtained. Calculated amounts of Nd and Cd were weighed on a semi-micro balance with an accuracy of at least ±0.5 mg.

The high reactivity of Nd with water and oxygen [24] as well as the high volatility of Cd restricts the number of materials that can be used for sample preparation. RE metals attack alumina and quartz glass largely at high temperature preventing their application. Tantalum had been found to be an ideal material. No intermetallic compounds are formed in the Nd–Ta system [20], and only a very slight pick-up of Ta by RE metals was reported by Spedding and Daane [25]. Dennison et al. [26,27] determined the very low solubility of Ta in liquid Nd only for high temperatures between 1547 and 2070 °C. The result of the assessment by Garg et al. [28] indicated a negligible (0.006 at.%) solubility of Nd in Ta at 1021 °C. In addition, a Ta crucible can be easily closed with a corresponding Ta lid by welding in a standard arc furnace [29] providing sufficient protection of the contained sample.

Therefore, all alloys were prepared in Ta crucibles (10 mm O.D., 15 mm height) which were closed by welding with a corresponding lid in a water-cooled arc furnace under an Ar pressure of 0.5 bar. The mass loss during the whole sample preparation procedure was usually below ±0.2 mg and did not significantly affect the sample composition. The total sample weight was usually 1 g, for dilatometric studies 2 g samples were prepared. The closed Ta crucibles were sealed separately in quartz glass tubes under 10^{-3} mbar and placed into a muffle furnace for various durations ranging from 3 to 12 weeks. Initially, all samples were melted for proper homogenization for at least 3 days; for samples containing ⩽70 at.% Cd a temperature of 1050 °C was selected which is slightly above the melting point of pure Nd, all other samples were kept at 700 °C. Afterward, different heat treatment steps were applied in the temperature range between 200 and 850 °C (see Table 3). The annealed samples were quenched in cold water and characterized by X-ray diffraction (XRD), light optical microscopy (LOM), energy dispersive X-ray spectroscopy (EDS) and differential thermal analysis (DTA). Additional dilatometric measurements were carried out for three Nd-rich samples.

Phase identification was done by powder XRD using Cu Kα radiation on a Bruker D8 Advance Diffractometer with Bragg–Brentano focusing geometry. For this purpose, sample pieces were powdered inside the glove box and afterward glued to a carrier by use of Vaseline dissolved in n-hexane. Special sample holders with X-ray transparent lids were used to prevent sample powders from oxidation. The XRD patterns were analyzed and refined by means of the TOPAS 3 software (provided by Bruker), applying the fundamental parameter approach for peak profile modeling.

For metallographic studies, pieces of the quenched samples were first embedded in a resin/carbon mixture, ground under paraffin oil or kerosene, polished with an oil-based diamond suspension and finally cleaned in an ultrasonic bath with n-hexane. With increasing Nd content the surface oxidation rate increased, hence, the polishing of samples containing more than 50 at.% Nd was more laborious and required a rapid transfer into the glove box. The quality of the polished samples was checked in a LOM (Zeiss Axiotech 100). In order to investigate microstructures and chemical compositions of the samples, a scanning electron microscope (SEM: Zeiss Supra 55 VP) with directly coupled EDS was applied. The measurements were performed at an acceleration voltage in the range of 15–20 kV. Pure Co acted as a standard to control parameters of the measured beam.

Differential thermal analyses were carried out on a DTA 404 S and DSC 404 PC as well as on a SETARAM Setsys Evolution, using Pt/Pt10%Rh thermocouples. The instruments were calibrated at the melting points of high purity metals: Ag, Cu, Ni and Zn. A sample mass of 100 mg was used for the experiments and high-purity γ-Al_2O_3 was employed as reference material. All samples, except pure Cd, underwent two heating and cooling cycles using a heating/cooling rate of 2 K min^{-1} (as-cast samples) and 5 K min^{-1} (annealed samples). They were contained in hermetically closed Ta-crucibles with plane bottoms (for better contact) which were formed using a hydraulic press. A constant Ar flow of 50 ml min^{-1} was applied in the DTA furnace chamber. The accuracy of the temperatures determined from the DTA curves is estimated to be better than ±2 °C.

Samples containing 1, 2, and 4 at.% Cd were also studied on heating and cooling by dilatometry using a horizontal dilatometer (Netzsch 402E) with inner tube diameter of 35 mm. The samples were prepared in closed Ta tubes (12 mm O.D., 35 mm long) and annealed at 200 °C. After an equilibration time of 12 weeks, the alloys were cut and precisely machined into the form of cuboids. In order to compare the DTA results with those from dilatometry, similar experimental conditions like heating and cooling rate (5 K min^{-1}) as well as an Ar flow of 50 ml min^{-1} were used.

3. Results and discussion

3.1. The equilibrium phase diagram

A total number of 70 samples were annealed and characterized by powder-XRD, SEM and DTA to obtain a complete description of the Nd–Cd phase diagram. Equilibrated samples and as-cast alloys were consulted to define homogeneity ranges, phase equilibria and crystallization behavior. Relevant samples, examined with isothermal methods, are listed in Table 2. Moreover, dilatometric measurements were performed to determine phase boundaries in the Nd-rich part (compare chapter 3.3.).

Based on the combined results from isothermal and dynamic methods as well as dilatometric measurements, a complete version of the Nd–Cd phase diagram was drawn, which is given in Fig. 1. All seven intermetallic compounds which were found in literature (Table 1) could be obtained in equilibrated samples. Lattice parameters and phase compositions of phases in relevant samples are listed along the complete composition range in Table 2. The corresponding phase boundaries of all intermetallic compounds as well as solid solutions are listed in Table 3 together with estimated homogeneity ranges from isopiestic vapor pressure measurements [30]. It is striking that the homogeneity ranges of all phases appear to be shifted toward the Nd-rich side of the nominal stoichiometry, something that had already been observed in other RE-Cd systems [4–7].

All experiments to obtain single-phase samples of the solid solutions of Nd by quenching failed. Although the solid solution of Cd in α-Nd could be clearly identified from the present EDX

Table 2
Experimental phase compositions and lattice parameters of equilibrium phases in selected Nd–Cd samples.

Sample/nom. comp. (at.%)	Annealing temp. (°C)	Phase analysis		SEM	
		Phases	Lattice parameters (Å)	Cd (at.%)	Nd (at.%)
1	300	Cd	a = 2.9794(5), c = 5.6194(1)	100	0.0
Nd_3Cd_{97}		$NdCd_{11}$	a = 9.3011(5)	91.6	8.4
2	300	$NdCd_{11}$	a = 9.2957(9)	91.3	8.7
$Nd_{11}Cd_{89}$		$NdCd_6$	a = 15.6285(2)	85.7	14.3
3	300	$NdCd_6$	a = 15.6318(1)	85.0	15.0
$Nd_{16}Cd_{84}$		$Nd_{13}Cd_{58}$	a = 15.6152(1), c = 15.4661(1)	81.6	18.4
4	600	$Nd_{13}Cd_{58}$	a = 15.6250(3), c = 15.4316(4)	–[a]	–[a]
$Nd_{19}Cd_{81}$		$Nd_{11}Cd_{45}$	Low intensity	80.5	19.5
5	600	$Nd_{11}Cd_{45}$	a = 21.7817(2)	79.2	20.8
$Nd_{23}Cd_{77}$		$NdCd_3$	a = 7.1692(3)	75.0	25.0
6	600	$NdCd_3$	a = 7.1792(4)	74.5	25.5
$Nd_{30}Cd_{70}$		$NdCd_2$	a = 5.0232(2), c = 3.4489(2)	66.6	33.4
7	850	$NdCd_3$	a = 7.1804(5)	75.3	24.7
$Nd_{28}Cd_{72}$		$NdCd_2$	a = 5.0231(4), c = 3.4474(4)	–[a]	–[a]
8	600	$NdCd_2$	a = 5.0255(4), c = 3.4440(3)	65.0	35.0
$Nd_{46}Cd_{54}$		NdCd	a = 3.8198(2)	50.6	49.4
9	850	$NdCd_2$	a = 5.0228(8), c = 3.4518(8)	65.5	34.5
$Nd_{37}Cd_{63}$		NdCd	a = 3.8204(5)	50.6	49.4
10	600	NdCd	Too ductile	47.4	52.6
$Nd_{70}Cd_{30}$		β-Nd	Too ductile	16.5	83.5

[a] The microstructure of the respective phase was too fine for an accurate measurement by EDX.

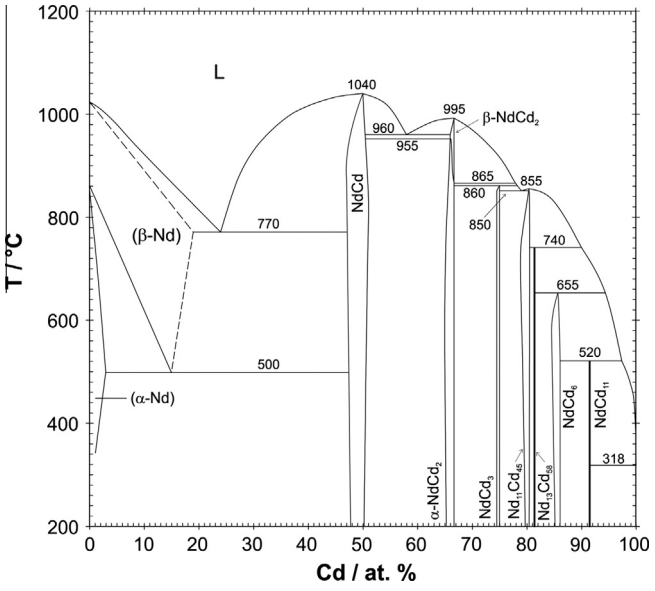

Fig. 1. The Nd–Cd phase diagram according to the present results.

results, minor amounts of unreacted Nd were always present. Similarly, the high-temperature modification β-Nd could be observed in quenched samples but most of the corresponding microstructures showed inhomogeneities.

Besides, XRD investigations showed the presence of unreacted Cd in some quenched samples with nominal compositions between 0 and 90 at.% Cd (cf. the pattern of sample $Nd_{37}Cd_{63}$ in Fig. 2). It has to be assumed that, due to rapid quenching of the sample, evaporated Cd condensed on the surface of the specimen. Therefore, the XRD pattern shows traces of Cd while the SEM micrograph does not. In fact, these relatively small amounts of Cd which had been evaporated and re-condensed on the sample surface on quenching did not significantly change the nominal compositions of the samples. Thus, the expected phase equilibria were reached in most of the samples which had been prepared with nominal compositions located in two-phase fields (see Table 2).

While most of the samples which contained intermetallic compounds turned out to be rather brittle, powdering of alloys containing the phases NdCd and $NdCd_2$ was very difficult due to their rather significant ductility. This is in agreement with observations in the related Gd–Cd system [31] where Vickers hardness measurements showed that the phases $GdCd_2$ and GdCd exhibited the lowest hardness values. Since $GdCd_2$ and GdCd are isotypic with the present compounds $NdCd_2$ and NdCd a similar mechanical behavior was to be expected and, in fact, observed. Consequently, the XRD-powder patterns of $NdCd_2$ and NdCd showed rather broad peak shapes. Additionally, absorption phenomena of these Nd-rich phases lowered also the intensities and made it altogether difficult to derive accurate lattice parameters.

3.2. Evaluation of isothermal and dynamic measurements

Samples studied by DTA are listed in Table 4, together with their thermal effects from two heating and cooling cycles, respectively. The temperatures for invariant effects in Fig. 1 are given as the average values from several independent measurements indicating error limits of ±5 °C or less. Generally, the results obtained for the as-cast samples are in good agreement with those for the annealed ones.

For each sample two heating and cooling cycles were performed at a heating rate of 2 K min^{-1} (as-cast samples) and 5 K min^{-1} (annealed samples) in order to check if equilibrium conditions can be restored after the first melting of the sample. Liquidus effects were evaluated both on heating and cooling if possible; all other effects were taken from the heating curves only. All invariant reactions, evaluated from the present results, are listed in Table 5 together with the respective reaction temperatures and types and the phase compositions. As can be seen, the intermetallic compounds $NdCd_{11}$, $NdCd_6$, $Nd_{13}Cd_{58}$ and $NdCd_3$ are formed incongruently whereas $Nd_{11}Cd_{45}$, $NdCd_2$ and NdCd show congruent melting behavior.

According to literature [11], the transition between α-Nd and β-Nd occurs at 862 °C, and the melting point of Nd is at 1024 °C [11] or 1021 °C [21], respectively. Attempts to reproduce these values gave inconclusive results: the α to β transition appeared to be at lower temperature, and the melting point was indicated at higher temperature; however the corresponding melting effect in

Table 3
Comparison of phase boundaries at different temperatures derived from SEM analyses and isopiestic vapor pressure measurements [30].

Compound	SEM		Isopiestic experiment	
	Temperature (°C)	Phase boundaries (at.% Cd)	Temperature (°C)	Phase boundaries (at.% Cd)
α-Nd	500	0–3.0	–	–
β-Nd	770	0–19.0	–	–
NdCd	300	47.8–50.0	550	48.7–50.1
	600	47.4–50.2		
	850	47.0–50.6		
$NdCd_2$	600	65.0–66.7	550	65.7–67.1
	850	65.5–66.7		
$NdCd_3$	600	74.4–75.0	–	–
	850	74.4–74.8		
$Nd_{11}Cd_{45}$	600	79.2–80.5	550	79.7–80.3
$Nd_{13}Cd_{58}$	300	81.4–81.7	550	81.2–81.7
	600	81.5–81.8		
$NdCd_6$	300	85.0–85.7	550	84.6–85.7
	600	84.6–85.6		
$NdCd_{11}$	300	91.3–91.8	–	–

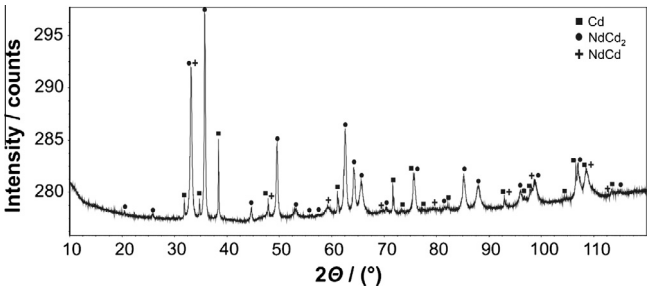

Fig. 2. The XRD pattern of the $Nd_{37}Cd_{63}$ sample annealed at 850 °C for 3 weeks.

the DTA resembled more a typical non-invariant effect than a clear DTA signal which one might expect from an invariant melting point of a pure substance. From this it must be concluded that the impurity content (probably most of it oxygen) of the Nd was still high enough to prevent the determination of a reliable melting point. Thus we kept the literature values for the α-Nd to β-Nd transition (862 °C) and the melting point of β-Nd (1021 °C) for the present phase diagram.

Extended solid solutions of Cd in both α-Nd and β-Nd were reported earlier [12,13] and could be confirmed in the present study. The respective solubility limits of Cd within Nd were determined at about 3 (α-Nd) and 19 at.% (β-Nd) in the present study (cf. Table 1). It was observed that Cd stabilizes β-Nd down to 500 °C were it decomposes in a eutectoid reaction forming α-Nd and NdCd. At 770 °C β-Nd is formed according to the eutectic reaction L = β-Nd + NdCd. The recorded DTA curve for the sample $Nd_{60}Cd_{40}$, annealed at 400 °C for 6 weeks, is given in Fig. 3. Both, the eutectoid and the eutectic reaction as well as the melting effect can be clearly distinguished. Nevertheless, the eutectoid reaction could not be observed in the heating and cooling curves of the sample $Nd_{55}Cd_{45}$. Most probably, the effect is already too weak due to an insignificant amount of α-Nd in the sample.

The compound NdCd melts congruently at 1040 °C and forms a eutectic (58 at.% Cd) with $NdCd_2$ at 960 °C: L = NdCd + $NdCd_2$. The microstructure of the sample $Nd_{46}Cd_{54}$, representing the structure of the eutectic between NdCd and $NdCd_2$, is shown in Fig. 4. NdCd shows a relatively broad homogeneity range. Its limiting compositions were determined as 47 and 50.6 at.% Cd at 850 °C (cf. Table 3).

For compositions between 54 and 77 at.% Cd some additional thermal effects were noticed in the temperature range 860–960 °C, most probably corresponding to the transformation of $NdCd_2$ into a high temperature modification (shown as β-$NdCd_2$ in Fig. 1). Such a polymorphic modification of $RECd_2$ intermetallic phases was already found in other RE-Cd systems, for example in the systems Gd–Cd [31] and Pr–Cd [4]. Unfortunately, all attempts to synthesize the high temperature modification β-$NdCd_2$ and retain it by quenching were unsuccessful. The intermetallic compound $NdCd_2$ has a congruent melting point at 995 °C and takes part in the peritectic formation reaction of $NdCd_3$ at 860 °C which is clearly observed by DTA for samples between 70 and 78 at.% Cd. For example, for the sample $Nd_{22}Cd_{78}$ two sharp DTA peaks were registered: the peritectic decomposition of $NdCd_3$ as well as the eutectic reaction between $NdCd_3$ and $Nd_{11}Cd_{45}$ at 850 °C and 79 at.% Cd. No separate liquidus effect could be recognized in this sample, neither on heating nor on cooling, which indicates that it must be very close to the peritectic reaction temperature.

The intermetallic compound $Nd_{11}Cd_{45}$ with a nominal composition of 80.4 at.% Cd melts congruently at 855 °C which is an average value of several independent DTA measurements. Metallographic examination of the sample $Nd_{22}Cd_{78}$, annealed at 600 °C for 4 weeks, showed the presence of both phases, $NdCd_3$ and $Nd_{11}Cd_{45}$ (Fig. 5). At this temperature $Nd_{11}Cd_{45}$ dissolves about 1 at.% Nd (cf. Table 3). This solubility was also indicated by isopiestic vapor pressure measurements [30].

It can be recognized that the liquidus curve decreases rather steeply between 80.4 and 100 at.% Cd. In this composition range, three consecutive peritectic reactions occur: at 740 °C the phase $Nd_{13}Cd_{58}$ is formed, followed by the peritectic formation of $NdCd_6$ and $NdCd_{11}$ at 655 and 520 °C, respectively. $NdCd_6$ showed a slight variation of the solubility of Nd with temperature and its homogeneity range is limited on the Nd-rich side at 84.6 at.% Cd at 600 °C. No significant solid solubility was determined for $NdCd_{11}$ which seems to be a line compound.

Similarly as reported by Johnson et al. [15], the liquidus temperature of an annealed sample with 5 at.% Nd could not be determined from the heating curve, however, it was observed during cooling. Nevertheless, for the as-cast sample Nd_4Cd_{96} it was clearly registered also on heating using a rate of 2 K min^{-1}.

In other RE-Cd systems, Bruzzone and Merlo [32] and Canepa et al. [33] indicated the tendency to supercooling for compositions between 3 and 15 at.% La or Ce, respectively. A similar tendency was also observed in this work, especially for sample compositions up to approximately 35 at.% Nd (see Table 4).

The shape of the liquidus curve between 97.4 and 100 at.% Cd was drawn following the extrapolation of the data listed in Ref. [15]. A strong invariant effect was noticed at 318 °C, which corresponds to the eutectic L = $NdCd_{11}$ + Cd. When extrapolating the equation, given by Johnson et al. [14], to the eutectic temperature, the eutectic point itself would be at 0.017 at.%. No significant solid solubility of Nd in Cd was detected by SEM in the present study.

Table 4
Experimental results of DTA in the Nd–Cd system.

Sample comp. (at.%)	Annealing T (°C)/weeks	Heating (°C)					Cooling (°C)
		Invariant reaction[a]				Phase boundary	Liquidus	Liquidus
$Nd_{99}Cd_1$	250/12					325 705–777	n-o	n-o
$Nd_{98}Cd_2$	300/10					613–809	1016	1015
$Nd_{95}Cd_5$	as-cast	498				n-o	970	968
$Nd_{95}Cd_5$	600/4	495				n-o	967	961
$Nd_{90}Cd_{10}$	as-cast	495				n-o	923	922
$Nd_{90}Cd_{10}$	800/3	502				n-o	914	913
$Nd_{88}Cd_{12}$	400/6	504				n-o	893	892
$Nd_{80}Cd_{20}$	as-cast	495	775				813	813
$Nd_{80}Cd_{20}$	400/6	498	773				804	803
$Nd_{78}Cd_{22}$	400/6	503	770				n-o	787
$Nd_{70}Cd_{30}$	as-cast	493	771				941	n-o
$Nd_{60}Cd_{40}$	400/6	504	769				1010	1004
$Nd_{55}Cd_{45}$	as-cast	n-o	765				1039	1033
		500 ± 5	**770 ± 5**				1018	1012
$Nd_{46}Cd_{54}$	as-cast	954	959				1030	1021
$Nd_{46}Cd_{54}$	400/6	950	957				1030	1023
$Nd_{37}Cd_{63}$	as-cast	955	961				991	990
$Nd_{37}Cd_{63}$	600/4	955	963				993	991
		955 ± 5	**960 ± 3**					
$Nd_{35}Cd_{65}$	600/4	n-o	866				992	965[sc]
$Nd_{30}Cd_{70}$	as-cast	864	n-o				964	950[sc]
$Nd_{26}Cd_{74}$	600/4	861	866				n-o	n-o
$Nd_{23}Cd_{77}$	as-cast	863	865	849			883	860[sc]
$Nd_{23}Cd_{77}$	600/4	860	**865 ± 1**	853			n-o	n-o
$Nd_{22}Cd_{78}$	600/4	859		852			n-o	n-o
		860 ± 4		**850 ± 3**				
$Nd_{19}Cd_{81}$	as-cast			n-o			853	834[sc]
$Nd_{16}Cd_{84}$	as-cast			738			843	812[sc]
$Nd_{16}Cd_{84}$	600/4			740			834	834
$Nd_{12}Cd_{88}$	as-cast	515	653	744			775	750[sc]
				740 ± 4				
$Nd_{10}Cd_{90}$	400/6	520	n-o				744	724[sc]
			655 ± 2					
Nd_7Cd_{93}	as-cast	520			316		n-o	650[sc]
Nd_5Cd_{95}	300/10	523			320		n-o	620[sc]
Nd_4Cd_{96}	as-cast	521			316		622	577[sc]
		520 ± 3			**318 ± 2**			

n-o not observed, sc supercooled effect.
[a] Average values of all invariant reaction temperatures are given together with estimated error limits in bold numbers.

Table 5
Invariant reactions in the system Nd–Cd derived from a combination of all present results.

Reaction	T (°C)	Phase compositions (at.% Cd)			Reaction type
$L \rightleftarrows Cd + NdCd_{11}$	318 ± 2	~100	~100	91.7	Degenerate eutectic
$L + NdCd_6 \rightleftarrows NdCd_{11}$	520 ± 3	97.4	85.9	91.7	Peritectic
$L + Nd_{13}Cd_{58} \rightleftarrows NdCd_6$	655 ± 2	94.4	81.7	85.7	Peritectic
$L + Nd_{11}Cd_{45} \rightleftarrows Nd_{13}Cd_{58}$	740 ± 3	89.9	80.4	81.7	Peritectic
$Nd_{11}Cd_{45} \rightleftarrows L$	855		80.4		Congruent melting
$L \rightleftarrows Nd_{11}Cd_{45} + NdCd_3$	850 ± 3	79.0	80.3	75.0	Eutectic
$L + \alpha\text{-}NdCd_2 \rightleftarrows NdCd_3$	860 ± 4	78.2	66.7	75.0	Peritectic
$\alpha\text{-}NdCd_2 \rightleftarrows \beta\text{-}NdCd_2$	865 ± 1		66.7		Polymorphic transformation
	955 ± 3		66.1		
$\beta\text{-}NdCd_2 \rightleftarrows L$	995		66.7		Congruent melting
$L \rightleftarrows \beta\text{-}NdCd_2 + NdCd$	960 ± 3	58.1	66.1	50.5	Eutectic
$NdCd \rightleftarrows L$	1040		50.0		Congruent melting
$L \rightleftarrows NdCd + \beta\text{-}Nd$	770 ± 5	24.0	47.2	19.0	Eutectic
$\beta\text{-}Nd \rightleftarrows NdCd + \alpha\text{-}Nd$	500 ± 5	15.0	47.5	3.0	Eutectoid

For the Cd-rich part of the phase diagram, the detected reaction temperatures were roughly comparable with values given in Ref. [20]: the peritectic decomposition of $NdCd_{11}$, reported at 530 °C in Ref. [20], was found here at 520 °C, and the eutectic between $NdCd_{11}$ and Cd was found at 318 °C instead of 321 °C in Ref. [20]. The value of 318 °C seems to be reasonable if compared with the published experimental data for the analogous eutectics in the Ce–Cd [33] as well as the Gd–Cd [31] systems, i.e. 315 and 316 °C, respectively.

For the annealed DTA samples, oxidation of the Ta-crucibles was observed after DTA measurements in cases when samples where heated above 1000 °C. Apparently, Ta behaved as a getter material for oxygen traces in the DTA furnace chamber. Selected Ta crucibles were sectioned and both surface and cross-section

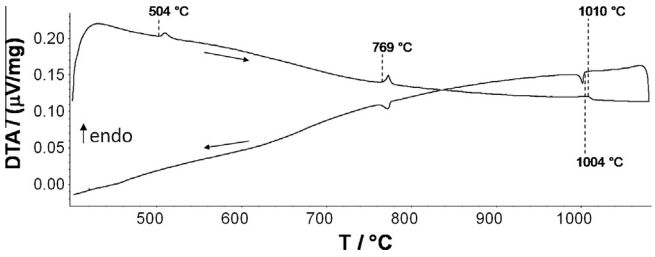

Fig. 3. DTA curves of the sample $Nd_{60}Cd_{40}$, annealed at 400 °C for 6 weeks, measured upon heating and cooling with 5 K min^{-1}.

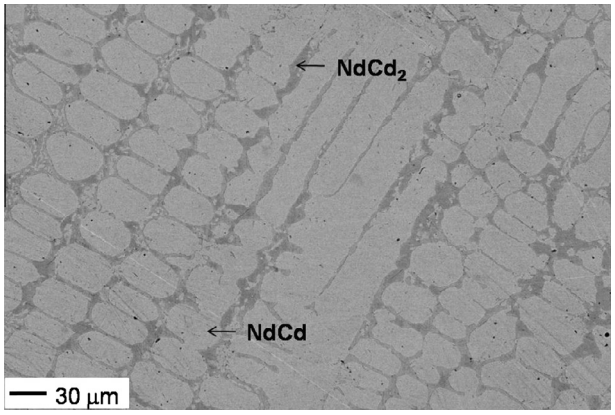

Fig. 4. Microstructure of the sample $Nd_{46}Cd_{54}$ annealed at 600 °C for 4 weeks.

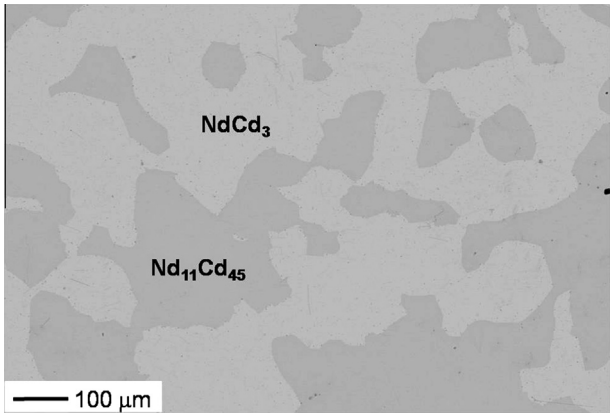

Fig. 5. Microstructure of the sample $Nd_{22}Cd_{78}$ annealed at 600 °C for 4 weeks.

were analyzed by SEM. Only minor amounts of Ta (up to 0.3 at.%) were observed in the corresponding samples, mostly in the part directly sticking to the crucible walls. It is assumed that this arises rather from a contamination during sample polishing than from a reaction of the sample with the crucible material itself.

3.3. Dilatometric study

Dilatometric curves display several effects observed upon heating of solid Nd–Cd samples. Although the signals of the recorded dimensional changes were weak, they nevertheless provided some additional information. Due to the high volatility of Cd only the following Nd-rich samples were investigated: $Nd_{99}Cd_1$, $Nd_{98}Cd_2$ and $Nd_{96}Cd_4$. The observed curve for the sample with 2 at.% Cd shows a similarity to the recorded DTA curve. It is presented in Fig. 6a, and the results can be summarized as follows:

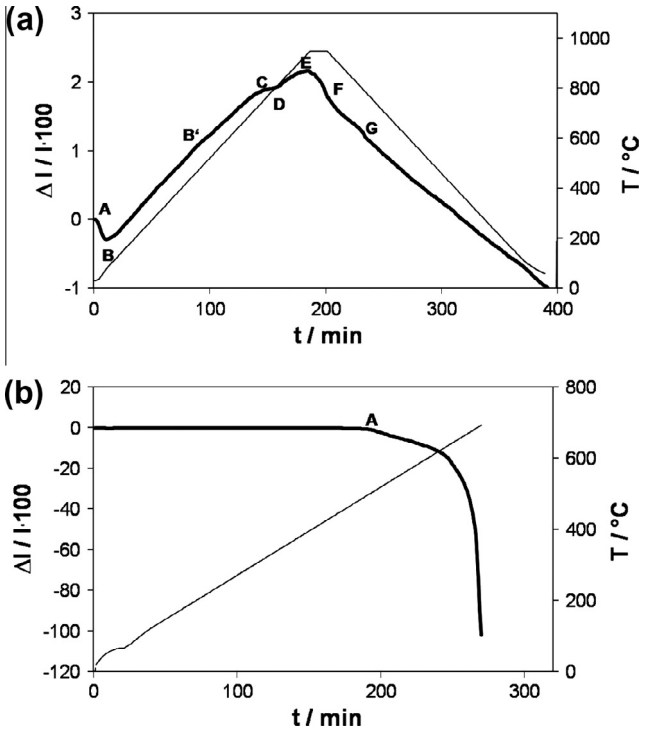

Fig. 6. Dilatometric curve (thick line) together with temperature curve (thin line) for the samples $Nd_{98}Cd_2$ (a) and $Nd_{96}Cd_4$ (b), recorded with a heating rate of 5 K min^{-1}.

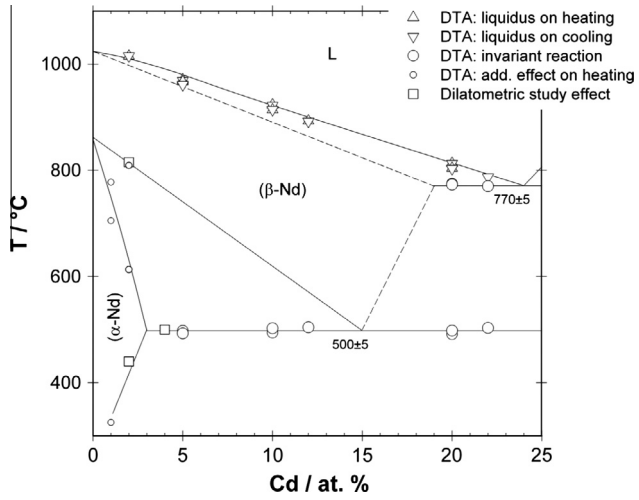

Fig. 7. Nd-rich part of the Nd–Cd phase diagram together with effects from DTA and dilatometry, recorded with a heating rate of 5 K min^{-1}.

(a) a sharp initial contraction (curve A–B);
(b) an expansion during heating with a slight maximum at about 440 °C (B′) corresponding to the phase boundary crossing α-Nd + NdCd → α-Nd (curve B–C);
(c) a decrease of the expansion rate between about 750 and 815 °C representing probably the transition into the two-phase field α-Nd + β-Nd (curve C–D);
(d) an increased expansion in the range between 815 °C and 950 °C (curve D–E);
(e) a shrinkage during the isothermal holding at 950 °C (curve E–F);
(f) a further contraction during cooling with a small effect (G) at about 810 °C which is probably connected to the phase boundary crossing β-Nd → α-Nd + β-Nd (curve F–G);

(g) a final contraction.

For the $Nd_{96}Cd_4$ sample the eutectoid reaction at 500 °C was indicated in the dilatometric curve during heating (A in Fig. 6b). DTA measurements of the latter sample did not show an effect which could be ascribed to the eutectoid reaction, probably because of the low sensitivity. A rather implausible contraction can be observed after point A in the dilatometric curve which was probably caused by a contraction of the sample during the eutectoid reaction which caused it to slip out of the specimen holder inside the dilatometer.

Fig. 7 shows the Nd-rich part of the Nd–Cd phase diagram with the effects recorded DTA and dilatometry (with a heating rate of 5 K min^{-1}). Obviously, these experimental data agree very well.

4. Summary

The Nd–Cd phase diagram was constructed using a combination of DTA, SEM, XRD and dilatometry data (Fig. 1). Cd solubilities in both α-Nd and β-Nd were determined and are listed in Table 1. Seven intermetallic compounds, described previously in literature, were confirmed and their phase boundaries were estimated by a combination of all available results. A congruent formation of NdCd, $NdCd_2$ and $Nd_{11}Cd_{45}$ was found whereas $NdCd_3$, $Nd_{13}Cd_{58}$, $NdCd_6$ and $NdCd_{11}$ decompose incongruently. The temperature values of the peritectic formation of $NdCd_{11}$ and of the eutectic between $NdCd_{11}$ and Cd were comparable with those given in Ref. [20], other invariant reaction temperatures had to be modified with respect to the literature values. Due to DTA results a polymorphic transition of $NdCd_2$ is proposed although the high temperature form β-NdCd could not be quenched. X-ray diffraction was used to confirm the crystal structure of all intermetallic compounds.

A dilatometric study was performed for Nd–Cd samples up to 4 at.% Cd. The results fit well with DTA data. α-Nd seems to have a higher thermal expansion than β-Nd.

Acknowledgements

This work was financially supported by the Austrian Science Fund (FWF) under Project No. P 23270-N19 as well as by the Scientific-Technical Cooperation Austria-India under Project No. IN 05/2011. The authors are grateful to Dr. Stephan Puchegger of the Faculty of Physics of the University of Vienna for his help and suggestions with the SEM measurements. The authors wish to thank Dr. Tadeusz Pieczonka from the AGH University of Science and Technology, Kraków, Poland, for his help with the dilatometric measurements.

References

[1] O. Conocar, N. Douyere, J. Glatz, J. Lacquement, R. Malmbecke, J. Serp, Promising pyrochemical actinide/lanthanide separation processes using aluminum, Nucl. Sci. Eng. 153 (2006) 253–261.
[2] D. Olander, Nuclear fuels – present and future, J. Nucl. Mater. 389 (2009) 1–22.
[3] M. Kurata, Y. Sakamura, T. Hijikata, K. Kinoshita, Distribution behavior of uranium, neptunium, rare-earth elements (Y, La, Ce, Nd, Sm, Eu, Gd) and alkaline-earth metals (Sr, Ba) between molten LiCl–KCl eutectic salt and liquid cadmium or bismuth, J. Nucl. Mater. 227 (1995) 110–121.
[4] T.L. Reichmann, H.S. Effenberger, H. Ipser, Experimental investigation of the Cd–Pr phase diagram, PLoS One 9 (4) (2014) e94025.
[5] B. Skołyszewska-Kühberger, T.L. Reichmann, R. Ganesan, H. Ipser, Thermodynamic study of the cerium–cadmium system, Calphad 44 (2014) 14–20.
[6] T.L. Reichmann, H. Ipser, Thermochemical investigations in the system cadmium–praseodymium relevant for pyro-metallurgical fuel reprocessing, Metall. Mater. Trans. A 45 (2014) 1171–1180.
[7] K.W. Richter, S. Besana, G. Borzone, H. Ipser, Thermodynamic investigations in the lanthanum–cadmium system, J. Alloys Comp. 365 (2004) 181–187.
[8] R.P. Elliott, Constitution of Binary Alloys, First Supplement, McGraw-Hill Inc, New York, 1985.
[9] A. Iandelli, Congr. Intern. Chim. Pure Appl., vol. 16, Paris, Mem. Sect. Chim. Minerale, 1958. pp. 35–40.
[10] A. Iandelli, Atti. Accad. Nazl. Lincei, Rend., Classe Sci. Fis., Mater. e Nat. vol. 29, 1960. pp. 62–69.
[11] K.A. Gschneidner, Rare Earth Alloys, D. van Nostrand Company Ltd, Canada, 1961.
[12] F.H. Spedding, A.H. Daane, W. Herrmann, The crystal structures and lattice parameters of high-purity scandium, yttrium and the rare earth metals, Acta Cryst. 9 (1956) 559–563.
[13] F.H. Spedding, J.J. Hanak, A.H. Daane, High temperature allotropy and thermal expansion of the rare-earth metals, J. Less-Common Met. 3 (2) (1961) 110–124.
[14] I. Johnson, in: J.F. Nachman, C.E. Lundin (Eds.), Rare Earth Research, Gordon and Breach Science Publishers Inc., New York, 1962, pp. 125–131.
[15] I. Johnson, K.E. Anderson, R.A. Blomquist, Partial constitutional diagram for the Cd–La, Cd–Ce, Cd–Pr, Cd–Nd, and Cd–Sm systems, Trans. Am. Soc. Met. 59 (1966) 352–355.
[16] I. Johnson, R. Schablaske, B. Tani, K. Anderson, Trans. AIME 230 (1964) 1485.
[17] A.C. Larson, D.T. Cromer, Acta Cryst. B27 (1971) 1875–1879.
[18] G. Bruzzone, M.L. Fornasini, F. Merlo, Rare earth intermediate phases with cadmium, J. Less-Common Met. 30 (1973) 361–375.
[19] A. Iandelli, R. Ferro, Alloys of cadmium with lanthanum, cerium and praseodymium, Gazz. Chim. Ital. 84 (1954) 463–478.
[20] T.B. Massalski, Binary Alloy Phase Diagrams, second ed., ASM International, Materials Park, Ohio, 1990.
[21] K.A. Gschneidner Jr., F.W. Calderwood, The cadmium-rare earth systems, Bull. Alloys Phase Diagrams 9 (1988) 16–21.
[22] C. Colinet, A. Pasturel, Thermodynamic properties of metallic systems, in: K.A. Gschneidner Jr., L.R. Eyring, G.H. Lander, G.R. Choppin (Eds.), Handbook on the Physics and Chemistry of Rare Earths – Lanthanides/Actinides: Physics – II, Elsevier Science B.V, Amsterdam, 1994, pp. 479–631.
[23] E. Veleckis, E. van Deventer, Eutectic temperatures in the LnCd–Ln fields of the lanthanon-cadmium systems, ANL-6925, Semi-Annual Report, July–December 1964, Argonne National laboratory, Argonne, IL, 1965.
[24] B.J. Beaudry, K.A. Gschneidner, Preparation and basic properties of the rare earth metals, in: K.A. Gschneidner Jr., L.R. Eyring (Eds.), Handbook on the Physics and Chemistry of Rare Earths – Metals – I, Elsevier Science B.V, Amsterdam, 1982, pp. 173–233.
[25] F.H. Spedding, A.H. Daane, Preparation and properties of rare earth metals, in: Progress in Nuclear Energy, I (5) Metallurgy and Fuels, 1956.
[26] D.H. Dennison, M.J. Tschetter, K.A. Gschneidner Jr., The solubility of Ta in 8 liquid RE metals, J. Less-Common Met. 10 (1965) 108–115.
[27] D.H. Dennison, M.J. Tschetter, K.A. Gschneidner Jr., The solubility of Ta and W in liquid RE metals, J. Less-Common Met. 11 (1966) 423–435.
[28] S.P. Garg, M. Venkatraman, N. Krishnamurthy, S.J. Vijaykar, The RE-Ta system, J. Phase Equilib. 19 (4) (1998) 385–394.
[29] Y. Janssen, M. Angst, P.C. Canfield, R.W. McCallum, Small sealed Ta crucibles for thermal analysis of volatile metallic samples, Rev. Sci. Instrum. 77 (2006) 056104. 1-056104_3.
[30] B. Skołyszewska-Kühberger, T.L. Reichmann, H. Ipser, A. thermodynamic study of the neodymium–cadmium system, 2014 (in preparation).
[31] G. Bruzzone, M.L. Fornasini, F. Merlo, The gadolinium–cadmium system, J. Less-Common Met. 25 (1971) 295–301.
[32] G. Bruzzone, F. Merlo, The lanthanum–cadmium system, J. Less-Common Met. 30 (1975) 303–305.
[33] F. Canepa, G.A. Costa, E.A. Franceschi, The phase diagram of the Ce–Cd system, Lanthanide Actinide Res. 1 (1985) 41–47.